University of Groningen

The temperature evolution of ultra-thin films in solid-phase reaction of Co with Si (111) studied by scanning tunneling microscopy

Ilge, B.; Palasantzas, Georgios; Nijs, J. de

[Link to publication in University of Groningen/UMCG research database](#)
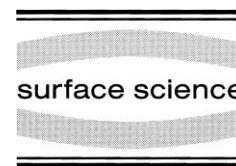
The temperature evolution of ultra-thin films in solid-phase reaction of Co with Si (111) studied by scanning tunneling microscopy

B. Ilge *, G. Palasantzas, J. de Nijs, L.J. Geerligs

Delft Institute for Microelectronics and Submicron Technology (DIMES) and Department of Applied Physics,
Delft University of Technology, NEXT-lab, Lorentzweg 1, 2628 CJ Delft, The Netherlands

Abstract

The solid-phase reaction of 5 Å of Co with the Si (111) surface is investigated by scanning tunneling microscopy (STM) in the range from room temperature to 700 °C. Room-temperature deposition leads to a granular film surface. The small grains transform upon annealing between 200 and 300 °C into triangular surface terraces with step heights of 1.5 and 3.1 Å. Further annealing up to 500 °C leads to their growth and a decrease of the relative number of 1.5 Å steps. These observations are explained by the formation of a cobalt silicide with a CsCl-type lattice. Furthermore, apart from the known 2×2 reconstructions and the unreconstructed surface, various surface features like individual double-line-shaped defects and steps with a height of 0.4 Å are resolved. Finally, the formation of pinholes is observed after annealing at 500 °C. They lead upon further annealing to a complicated pinhole-induced $CoSi_2$ network that breaks up into individual islands at ~ 700 °C. © 1998 Published by Elsevier Science B.V. All rights reserved.

Keywords: Epitaxy; Growth; Scanning tunneling microscopy; Silicides; Solid-phase epitaxy

1. Introduction

During the last two decades, a significant amount of effort has been devoted to the fabrication of defect-free $CoSi_2$ films with well-defined surfaces and interfaces [1,2]. This effort was largely motivated by the applicability of $CoSi_2$ films in microelectronic devices (gates, source and drain contacts, etc.) because of its low resistivity and small lattice mismatch with Si. For the film fabrication, the most widely used methods are molecular beam epitaxy (MBE), reactive deposition epitaxy

(RDE) and solid-phase epitaxy (SPE). In SPE, a metal film is deposited at room temperature on the Si surface, and the silicide film is formed by annealing at an elevated temperature. The latter method is of special interest because of its application in the salicide (self-aligned silicide) technique. Studies of the solid-phase reaction in SPE of films with thicknesses from tens of nanometres to micrometres showed the crucial role of material transport in the film [3,4], whereas the underlying diffusion mechanisms still remained poorly understood [5]. To reduce the influence of material transport, amorphous $CoSi_2$ was studied [6–8] in which both reaction partners co-exist in stochiometry at the growth front and diffusion is relatively unimportant.

---

* Corresponding author.
E-mail: ilge@cerberus.dimes.tudelft.nl

For ultra-thin (<10 Å) Co films, the mechanisms governing the solid-phase reaction are expected to be different from the above [9]. Whereas the Si is already present in the crystalline form, the structural form of the deposited metal depends on its reaction with the Si substrate. It was found that the first few (1–4) monolayers (ML) of Co already react with the Si substrate at room temperature (RT) to form an epitaxial layer [1,2,10–13] that, upon annealing, transforms into an epitaxial $CoSi_2$ film. The latter can be employed as a template on which further epitaxial growth of $CoSi_2$ can commence to form thicker films ("template technique") [1]. None the less, the nature of the epitaxial phase formed at room temperature is still under discussion [12,13]

Although these films have been studied with a variety of different experimental techniques [12–17], little has been done with scanning tunneling microscopy (STM), which can give local surface information down to the atomic level. Using STM, Bennett et al [18–20] studied the reaction of sub-monolayer to 2 ML coverages of Co deposited on substrates held at elevated temperatures (reactive epitaxy, RE), which did not lead to a closed film. Because of the low coverage and the elevated temperature, the kinetics and nucleation are expected to be quite different from those in a film geometry.

To enhance a further understanding of solid-phase epitaxy (SPE) mechanisms, we therefore present here an ultra-high vacuum STM study of the temperature evolution of an ultra-thin film of Co on Si (111). We chose a film thickness of 5 Å for which 1–2 ML of unreacted material are expected to be present on the film formed at RT [14,16,21]. This enables us to study the interaction of the unreacted material with the RT film as well as the transformation of the RT film to $CoSi_2$ with a CaF_2 lattice. In addition, this study is meant to be helpful for application of $CoSi_2$ in nano-electronic devices [22] where co-deposition of Co and Si is not the method of choice [23].

2. Experimental

Samples from a Si(111) wafer were degassed at 500 °C for several hours and flashed for a few minutes (<10 min) at 1200 °C, using resistive heating. The base pressure in the preparation chamber was 1×10^{-10} mbar, and the pressure was 5×10^{-9} mbar at the end of the high-temperature flash. The samples were then transferred into an STM chamber with a base pressure of 2×10^{-10} mbar. Mechanically prepared Pt/Ir tips were used. The z-piezo was calibrated with an uncertainty of 0.8% or less and checked between various measurement sets.

The clean surfaces showed perfect 7×7 reconstruction with 43(3)-nm-wide surface terraces. (The number in parentheses gives the accuracy of the last digit. Thus, $4.35(13) = 4.35 \pm 0.13$.) This is in good agreement with the independently measured miscut angle of $0.44(5)°$, determined using the method described by Stäuble-Pümpin et al. [24], which would result in an average terrace width of 41(4) nm. A 0.5(1)-nm-thick Co film was deposited at a deposition rate of 0.1 nm min^{-1} with an e-beam evaporator calibrated with a quartz crystal monitor. The pressure during evaporation did not rise above $\sim 5 \times 10^{-9}$ mbar. The sample temperature was monitored using an optical pyrometer for temperatures above 400 °C, and with a removable Pt/Rh (R-type) thermocouple at lower temperatures.

3. Results

After the RT deposition of Co, the step structure of the substrate is conserved and small grains with a diameter between 1 and 3 nm and a corrugation of 2.6(9) Å are found on the film surface (Fig. 1a). They lead to a root mean square (RMS) roughness on the terraces of 0.73 Å.

After annealing for a few minutes at temperatures between 200 and 300 °C, the grains transform partly into triangular islands (Fig. 1b) with the edges parallel to the $\langle 1$-$10 \rangle$ directions. Height measurements showed height differences between neighbouring terraces of 1.5(1) and 3.1(1) Å.

Subsequent annealing at 400 °C (Fig. 1c) leads to lateral growth of the triangular islands. Step heights of mainly 3.16(21) Å, and some of 1.54(16) Å were found. These step heights are in good agreement with the values for 1/3 and 1/6 of the $\langle 111 \rangle$ space diagonal for the bulk unit cell (uc)
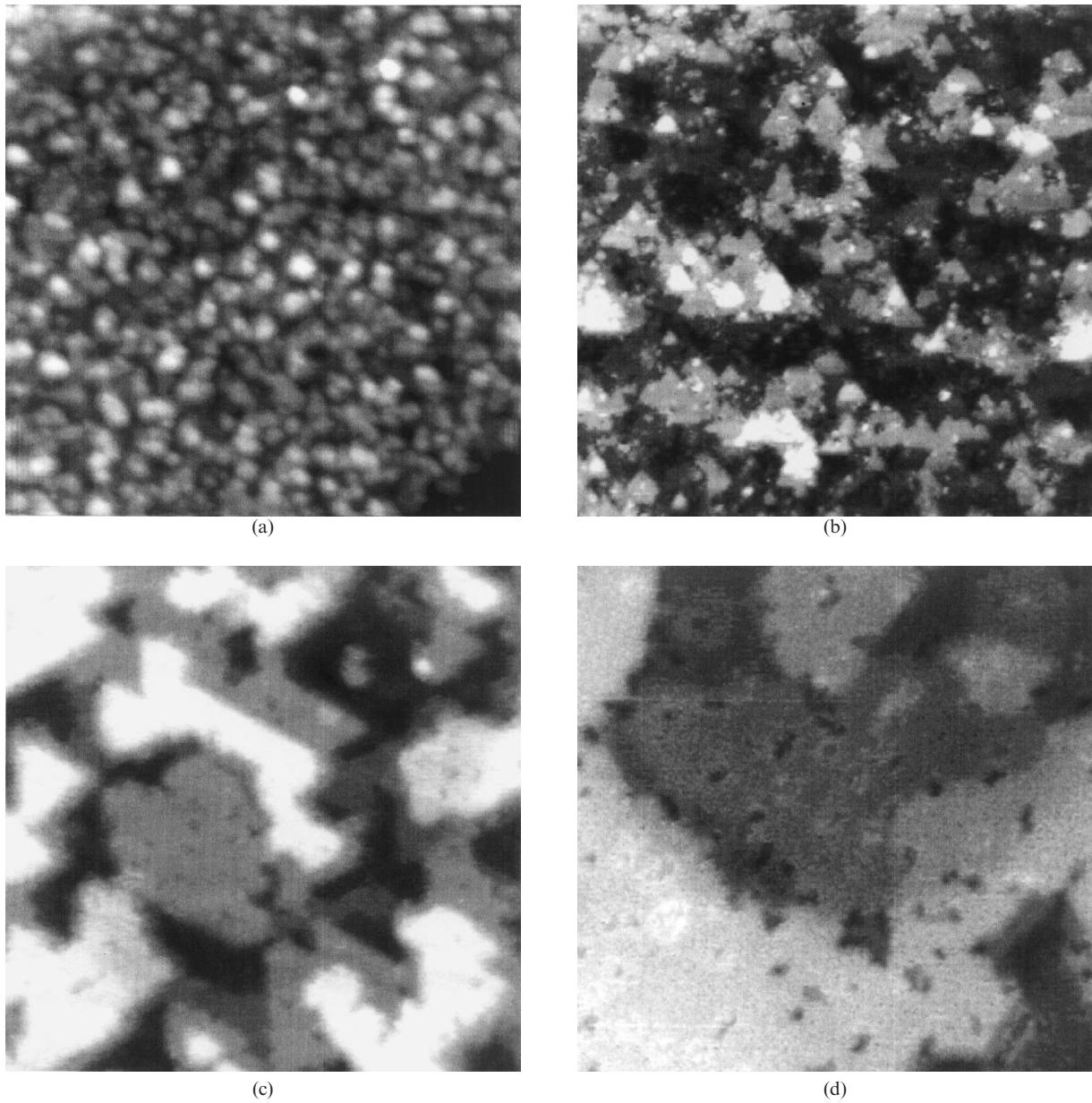
(a)

(b)

(c)

(d)

Fig. 1. STM image of a sample after consecutive anneal steps. Size for all images: 50×50 nm: (a) after deposition of 5 Å Co at room temperature; $V_{tip} = 1.55$ V; $I = 0.16$ nA; (b) after 3 min of annealing at 270 °C; $V_{tip} = 2.24$ V; $I = 0.87$ nA; (c) after 3 min of annealing at 400 °C; $V_{tip} = 1.28$ V; $I = 2.47$ nA; and (d) after 3 min of annealing at 500 °C; $V_{tip} = 2.61$ V; $I = 2.47$ nA.

of $CoSi_2$, which are 3.097 and 1.549 Å. In addition, after annealing at 400 °C small holes with diameters of 2.4(4) nm and a depth of 1.1(4) Å were found at a density of 2×10^4 μm^{-2}.

For samples annealed at 500 °C for 3 min (Fig. 1d), a variety of step heights appear, and only a few steps could still be identified as the 1/6 $\langle 111 \rangle$ uc type. Surprisingly, besides 1/3 and 1/6 $\langle 111 \rangle$ uc steps, we found clear steps with heights of 0.40(4) Å (Fig. 2). Small holes are still present,
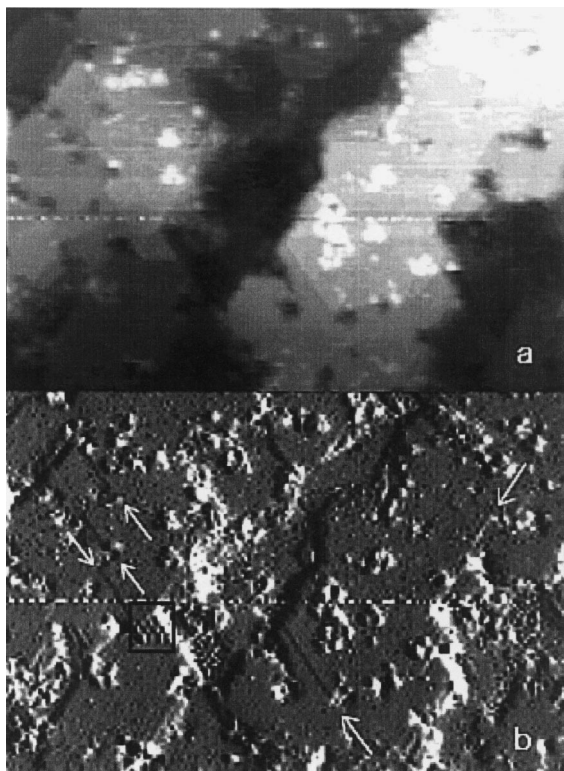
Fig. 2. STM image after 3 min annealing at 500 °C. (a) Height image and (b) current image of the same area. The white arrows in the current image mark surface steps with heights of 0.40(4) Å. The areas on top of such steps (α-surface) show decorations of the small holes with a trigonal shape. The areas at the bottom (β-surface) show no such decorations. The black box marks a 2 × 2 domain in front of a 1/6 ⟨111⟩ uc step; size: 48 × 33 nm; V_{tip} = 0.98 V; I = 1.02 nA.

tively high tunnel currents and low gap voltages were required.

The 2 × 2 reconstructed domains that appear preferentially in front of 1/6 ⟨111⟩ steps showed a corrugation amplitude of 0.75 Å (Fig. 3b). The highest points of the 2 × 2 areas were nearly of the same height as the upper terrace. In contrast to the 1 × 1 areas, the 2 × 2 domains were sensitive to scanning and degraded upon consecutive image scans. The 2 × 2 domains were not found on samples annealed at 400 °C, had a typical size of 70–40 protrusions after annealing at 500 °C, less than 10 after 550 °C, and finally disappeared after annealing at 600 °C. Although the 2 × 1 reconstruction reported earlier for co-deposited CoSi$_2$ [25] was not observed on samples annealed at 500 °C, individual double-line-shaped defects running parallel to the ⟨−110⟩ directions were observed (Fig. 3c). The distance between the two lines was found to be 6.5(9) Å. This is in good agreement with the length of the long diagonal of the surface unit cell and the distance between two rows of a 2 × 1 reconstruction, viz. 6.7 Å.

On the samples that had been annealed at 400 or 500 °C, areas were found that appeared to have a slope of 2.0° over a lateral length of 5(2) nm. The majority of these areas are found at the edges of terraces, and they seem to be closely related to the steps with 1/6 ⟨111⟩ uc heights.

After 3 min of annealing at 500 °C, the first pinholes were formed at a number density of 44(6) μm^{-2}, diameters of 38(7) nm and depths of 5.4(6) nm (Fig. 4). The bottoms of the pinholes appear to be flat and are often covered with grains. Subsequent annealing leads to the development of a complicated pinhole-induced network, which, at temperatures around 700 °C, breaks up into individual crystallographically oriented islands (Fig. 5). The surfaces of these islands appear, from the STM images, to be perfectly flat and rather featureless.

4. Discussion

4.1. Surface steps

The main result of this study concerns the development of the cobalt silicide film. A careful

with a diameter of approximately 2.7(6) nm, a depth of 3.1(9) Å and a density of 4.3(3) × 10^4 mm^{-2}. Similar to the holes of the sample annealed at 400 °C, their edges are often decorated with small protrusions 1.9(2) Å high and 1.3(4) nm wide. We note a higher density of these decorations on the higher of the two terraces forming 0.4 Å steps.

Furthermore, on samples annealed at 500 and 550 °C, we were able to resolve the 1 × 1 and 2 × 2 surface reconstructions that were described earlier for co-deposited films of CoSi$_2$ [25]. Fig. 3a shows an image of the 1 × 1 surface in the vicinity of a small hole. The measured corrugation amplitude is 0.23 Å. In order to resolve this structure, rela-
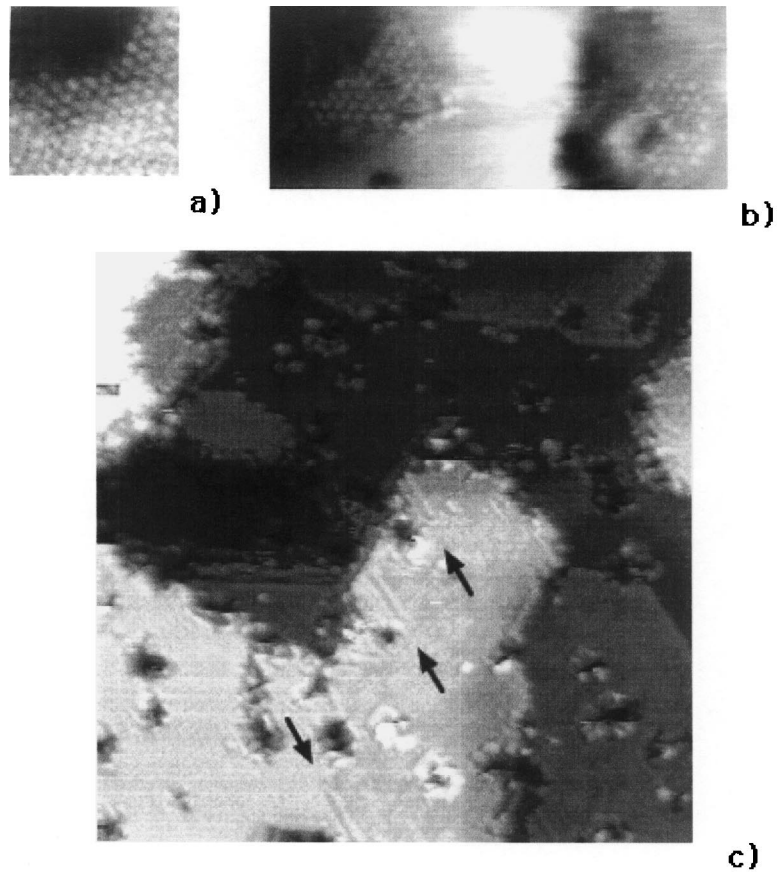
Fig. 3. STM image after 3 min. annealing at 500 °C. (a) 1×1 corrugation shown at the edges of one of the small holes with a corrugation amplitude of 0.23 Å. Size: 4×4 nm; $V_{tip} = 0.63$ V; $I = 4.93$ nA. (b) Two 2×2 reconstructed domains. The left domain sits at the bottom of $1/6 \langle 111 \rangle$ uc step (not visible), and the right domain contains one of the small holes. Both show a corrugation amplitude of 0.75 Å. Size: 25×10 nm; $V_{tip} = 0.27$ V; $I = 2.47$ nA. (c) The double-line-shaped surface defects and the bending of surface planes can be seen. The double-line-shaped defects show a corrugation of 0.24(4) Å and a spacing of 6.5(9) Å. Size: 35×35 nm; $V_{tip} = 0.98$ V; $I = 1.02$ nA.

analysis of step heights will be very useful in the interpretation. For bulk $CoSi_2$ on $\{111\}$ surfaces, only step heights of integer multiples of $1/3$ of the $\langle 111 \rangle$ uc would be expected, which corresponds to 3.097 Å. Thus, in order to understand the formation of step heights in integer multiples of $1/6$ of the $\langle 111 \rangle$ uc, we will discuss various possibilities that include different termination layers, anti-phase boundaries and possible electronic influences.

4.1.1. Termination layers

Fig. 6a shows the possible bulk terminations of $CoSi_2$ (B, C, D) and the Si-rich termination (A),

which was found on longer-annealed $CoSi_2$ surfaces [26]. Indeed, different combinations of the termination layers can lead to different step heights. As an example, we show in Fig. 6b the step heights for surfaces with adjacent Si-rich and Co-rich termination layers, which are found on thicker $CoSi_2$ films [1]. Such surfaces can only have step heights of $1/12$ (0.774 Å), $1/4$ (2.323 Å), $1/3$ (3.097 Å) $\langle 111 \rangle$ uc or higher. Therefore, they cannot explain the measured step heights of 1.5(1) Å.

The table in Fig. 6c shows the step heights for all possible combinations of the four termination layers. Surface steps with a height of $1/6 \langle 111 \rangle$ uc
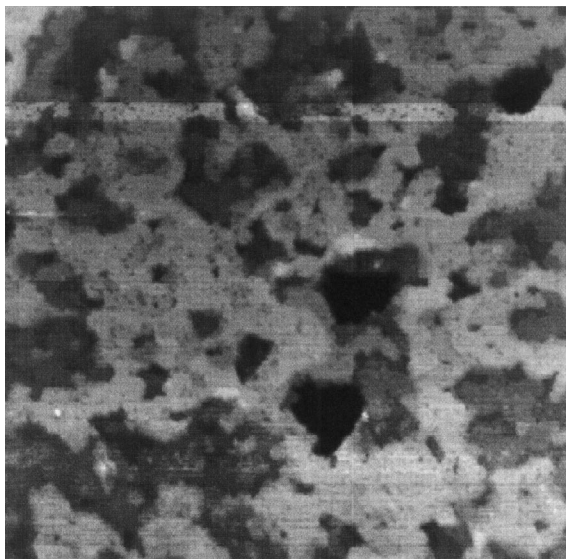
Fig. 4. STM image after 3 min of annealing at 500 °C, pinhole formation takes place. The grey scale covers a height difference of 1.3 nm. The bottom of the pinholes is not visible in this image. Size: 300 × 300 nm; $V_{\text{tip}} = 1.56$ V; $I = 1.56$ nA.
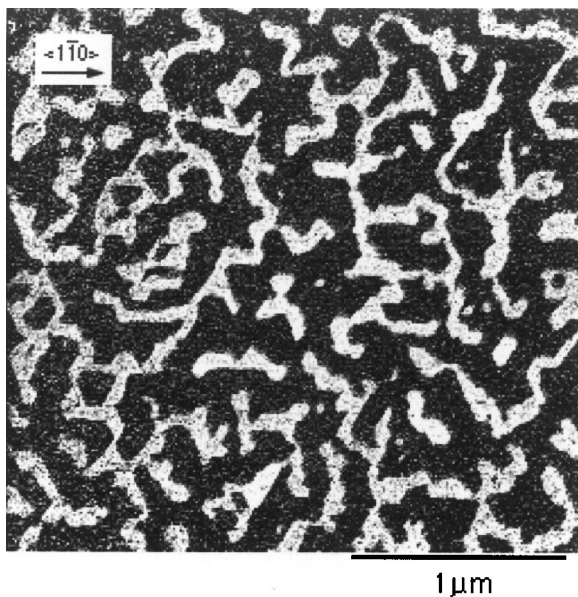

Fig. 5. SEM image (plane view, 30 kV) after annealing at 700 °C for 3 min. The pinhole-induced network breaks the film up into individual islands. The bright areas consist of $CoSi_2$, and the areas in-between of Si substrate (in STM 7×7 reconstructed).

(1.55 Å) could only result from the coexistence of B and C terminations. Whereas the C termination is found on $CoSi_2$, termination B still remains unverified [27–29]. Termination B is, in fact, very unlikely because the top Si atoms sit in an adatom-like position and have three dangling bonds, whereas the Si atoms in the second layer with their three fold co-ordination would, moreover, have a dangling bond. Such a high density of unsaturated chemical bonds would result in an energetically highly unfavourable surface which therefore is very likely to reconstruct. Bennett et al. suggested a Si-adatom model for the 2×2 reconstruction [20], which is a possible candidate for such a recon-structed B termination.

Areas with different surface reconstructions could also give rise to geometrical height differ-ences, possibly in combination with effects due to differences in the density of surface states. For example, the 2×2 reconstructed domains appear to be nearly 1/6 $\langle 111 \rangle$ uc higher than the 1×1 areas. However, none of the areas with 1/6 $\langle 111 \rangle$ uc height differences is 2×2 reconstructed, except the small domains that are sometimes found at such step edges. (Figs. 2 and 7).

4.1.2. Anti-phase boundaries

Another mechanism that can, in principle, create surface steps other than those expected for bulk $CoSi_2$ is the presence of anti-phase boundaries (APB). To form such an anti-phase boundary, a vertical displacement between the two sides of the boundary is needed with $\Delta z = \delta$ 1/3 $\langle 111 \rangle$ uc, where δ is a non-integer number. However, there are restrictions for the presence of APBs. APBs have to terminate on dislocation lines with a screw component (except for such trivial cases as ter-mination on the boundaries of the sample, on segregations of second phases or on other APBs). The Burgers vector of such dislocation lines would have a component perpendicular to the surface of Δz [30,31]. Every step with 1/6 $\langle 111 \rangle$ uc heights (which would then represent an APB underneath) would therefore appear as a pair of screw disloca-tions on the sample surface. This was not observed on our samples.

Whereas simple dislocations cannot create sur-face steps in the absence of APBs, they can contrib-

a)

termination A, Si rich termination   termination C, Co rich termination

termination B   termination D

b)

A-C step   C-A step

1/4 <111>

1/12 <111>

c)

lower area \ higher area	A	B	C	D
A	1/3	1/4	1/12	1/3
B	1/12	1/3	1/6	1/12
C	1/4	1/6	1/3	1/4
D	1/3	1/4	1/12	1/3

Co: ●
Si: ○

<111>

<11$\bar{2}$>

<1$\bar{1}$0>
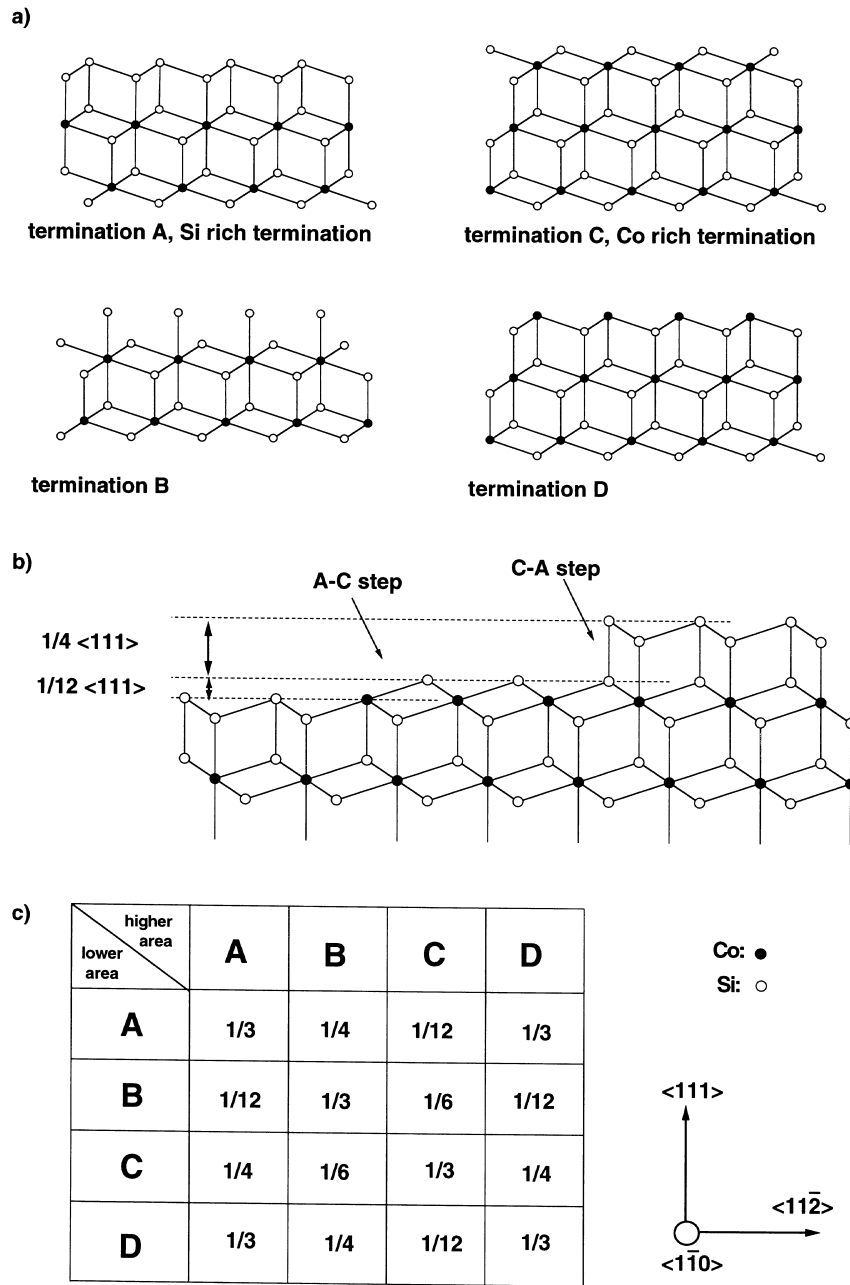
Fig. 6. Possible influence caused by different termination layers. (a) Projection along the $\langle 1\text{-}10 \rangle$ direction of the different surface termination layers. In addition to the three bulk-derived terminations B, C and D, the Si-rich termination layer A is shown. (b) Resulting step heights from the coexistence of the two experimentally found termination layers A and C. (c) Table of all possible step heights between the four different termination layers.

Fig. 7. Sample annealed at 500 °C for 3 min. Surface profile along a line close to the ⟨11-2⟩ direction. From left to right: β-surface, Islan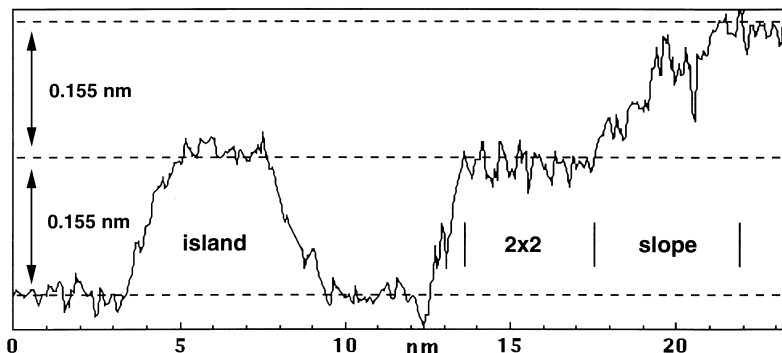d (with β-surface), β-surface, 2×2 reconstructed domain, sloped surface (with untypical high noise), β-surface. $V_{tip} = -0.063$ V; $I = 4.17$ nA.

ute to contrast in STM [32]. Stalder et al. found that misfit dislocations at the film/substrate interface give rise to height differences with a Lorentzian shape. However, this can explain neither the observed surface steps nor the observed bending of surface planes on our samples since the maximum height differences induced by such a mechanism will be a factor of two smaller than that which we observed.

4.1.3. Electronic effects

Kubby et al. showed recently that effects other than differences in the density of surface states (induced by different surface terminations or surface reconstructions) or height differences could give rise to contrast in the STM [33–35]. Films that are thin on the scale of the Fermi wavelength of the charge carriers can be described as two-dimensional conductors, where the quantization of the k-vector perpendicular to the film surface gives rise to thickness-dependent peaks in the density of states [33–35]. For a 2 nm film, the peak distances are in the order of several tenths of an electron-volt, which makes it possible to detect steps at the film/substrate interface. Although such an effect depends strongly on the energy of the tunneling electrons, the step heights of 1/6 ⟨111⟩ uc observed in our study are independent of the applied gap voltage. Therefore, we conclude that the measured step heights of 1/6 ⟨111⟩ uc cannot be attributed to electronic effects.

4.1.4. Modelling of the step heights

Regarding the above discussion, we believe that none of the previous mechanisms can explain the observed step heights. We think, therefore, that the assumption that the films consist of single-phase $CoSi_2$ (CaF_2 type) is incorrect. Indeed, it has been shown recently that epitaxial cobalt silicide films can grow in phases other than the well-known bulk phases [36–39]. The structure of the cubic CoSi with a CsCl lattice [36] can be derived by filling every octahedral interstitial site of the CaF_2-type $CoSi_2$ with an extra Co atom (see Fig. 8). By randomly taking out individual Co atoms from such a CsCl-type CoSi, one can derive the more general structure of the $CoSi_x$ "phase" ($1 \leq x \leq 2$) [37,38] (Fig. 8b). Both types of films can be grown by MBE deposition on CaF_2-type $CoSi_2$ template films. In fact, Hong et al. showed that such a $CoSi_x$ phase even forms via the direct solid-phase reaction of Co with CaF_2-type $CoSi_2$ at 350 °C [38,39].

Because we deposited 5 Å (5.7 ML) of Co, some unreacted Co would be expected to exist on top of the RT film [11,14], which on our samples shows up as the small grains. This is in agreement with the absence of LEED patterns for comparable samples [16,21]. If one assumes that the RT film consists of a CaF_2-type $CoSi_2$, upon further annealing, the reaction with the material on the film surface should lead to the same results as the experiments of Hong et al., and thus to a CsCl-derived Co-silicide phase at the sample surface.

Si unit   **CsCl type CoSi unit**

Si unit cell   **CoSi2 unit cell**   **8 CsCl type CoSi unit cells**

a)

CoSi$_2$ CoSi$_x$ CoSi

<111>

<1$\bar{1}$0>
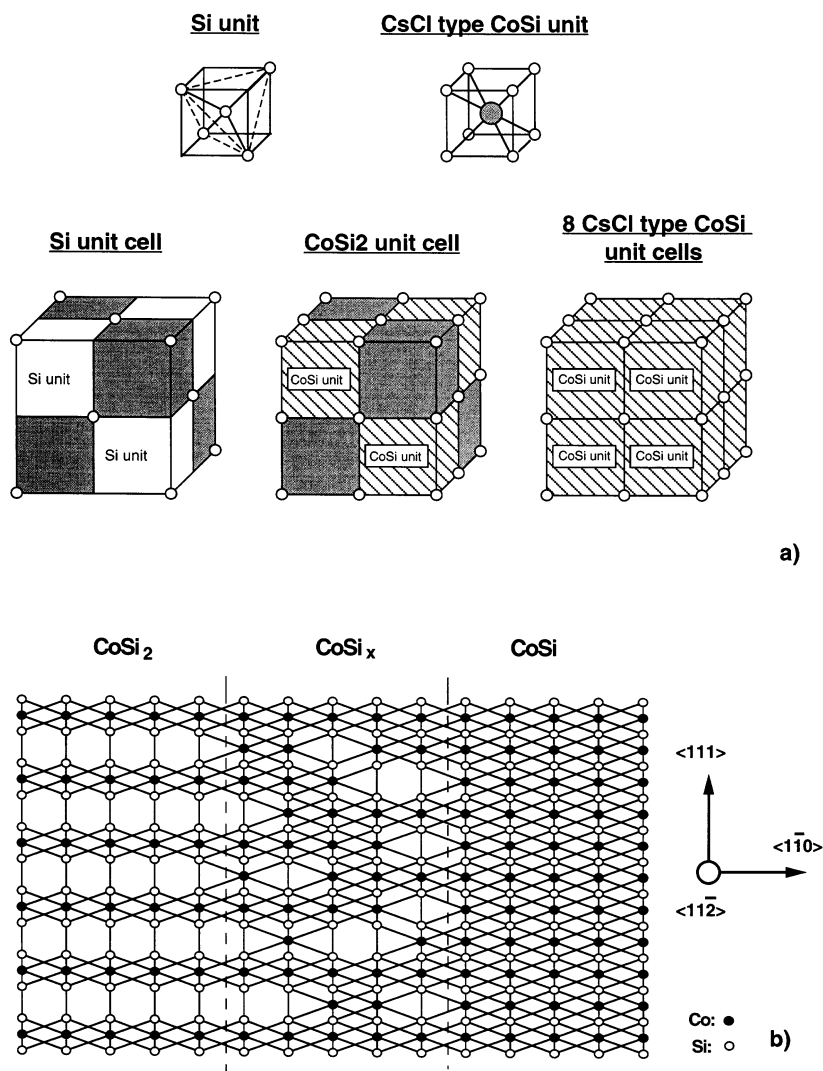
<$\bar{1}$1$\bar{2}$>

Co: ●   Si: ○   b)

Fig. 8. Different phases found for the solid-phase reaction of ultra-thin Co films on Si(111). (a) Shows the different unit cells with growing Co concentration from left to right. They consist of either Si or CoSi units combined with "empty" volumes (grey boxes). (b) To illustrate the structural changes during film evolution on a (111) surface, a projection along the $\langle 11\text{-}2 \rangle$ direction of the CaF$_2$ type CoSi$_2$, the CsCl-derived CoSi$_x$ and the CsCl type CoSi are shown.

On a (111) surface of such a CsCl-type CoSi, the heights of the surface steps are multiples of 1.58 Å, which is equal to our measured step heights of 1.5(1) Å. The (111) surface atomic plane of such a CsCl-derived cubic CoSi is identical to that of the Co-rich termination (termination C in Fig. 5a) of the CaF$_2$-type CoSi$_2$. The CsCl-type CoSi structure differs from the CoSi$_2$ at a depth of 1/4 $\langle 111 \rangle$ uc where the octahedral sites of the

CoSi$_2$ unit cells are occupied by an extra Co atom (Fig. 8b). Whereas the lattice parameter of the CaF$_2$-type CoSi$_2$ is 5.364 Å, i.e. 1.2% smaller than the one of Si, the cubic CsCl-type CoSi has a lattice parameter of half of 5.48(4) Å, which is 0.9% larger than that of Si. Moreover, Pirri et al. [37] found that the lattice parameter of CsCl-derived CoSi$_x$ decreases with increasing Co content. This suggests that because of the smaller

strain energy, $CoSi_x$ (with $1 < x < 2$) is energetically favoured to form during the initial stages of solid-phase reaction.

Therefore, we believe that the measured step heights can be explained by the presence of a CsCl-derived cubic cobalt silicide phase. This also explains the reduction in number of $1/6 \langle 111 \rangle$uc steps at higher annealing temperatures, and the bending of the surface planes that appears after annealing at 400 °C. On samples annealed at 500 °C, only a few steps could still be identified to be of the 1/6 type, and they totally disappeared after annealing at 600 °C. On annealing, Co atoms will diffuse from the upper part of the film to the interface with the Si leaving octahedral vacancies behind. Re-ordering has to occur so that during the evolution process, the layered structure of the CaF_2-type $CoSi_2$ can be formed (Fig. 8b). During such an ordering process, the surface steps also have to transform from the heights expected for CsCl-type CoSi to the heights characteristic of the CaF_2-type $CoSi_2$.

4.2. Additional features on samples annealed at 500 °C

After annealing at 500 °C, a variety of other surface features are found, such as additional steps with heights of 0.40(4) Å, 2×2 reconstructed domains, and double-line-shaped defects that all disappear upon annealing at 600 °C. They are most likely related to the transition from Co-rich to Si-rich surface termination that occurs at this temperature. This is consistent with LEED studies that showed that the 2×2 reconstruction took place during the surface transition [40].

These additional features are found to be accompanied by the formation of pinholes. Whereas the mechanisms leading to their formation remain unclear, pinholes enable the Si to reach the film surface more easily via surface diffusion rather than via the bulk of the silicide film where Co has been shown to be the major mobile species [41]. In this manner, the film surface can reach its equilibrium configuration much faster. We find indeed that our pinholes are more than 3 nm deeper than the expected film thickness of 1.8(7) nm for a fully reacted $CoSi_2$ film.

Comparable findings were reported for pinholes in co-deposited films [25], where the pinholes were found to be up to four times deeper than the thickness of the silicide film. From size, depth and density of the pinholes, one can calculate the total amount of Si transported through the pinholes to the film surface, which leads to 8.8 ± 6.4 Si atoms nm^{-2}. In comparison, for the transformation of the Co-rich to the Si-rich terminated surface, 15.66 Si atoms nm^{-2} are required. This suggests that much of the Si necessary for the surface transition is supplied by the pinholes.

Because we find steps with $1/6 \langle 111 \rangle$ uc height (Fig. 7) in co-existence with 2×2 domains, we believe that the surface transition from Co-rich to Si-rich termination already takes place, while the transition from CsCl-type to CaF_2-type silicide is not yet fully completed. The small steps of 0.40(4) Å lead to two different types of surfaces. We refer to the surface on top of such a step as an α-surface (which shows a higher density of decoration of the small holes) and that at the bottom of the step as a β-surface. 2×2 domains show on a β-surface the same height 1.5(1) Å as $1/6 \langle 111 \rangle$ uc (Fig. 6), whereas they show a height of 1.1(1) Å on an α-surface. The origin of the 0.4-Å steps stays unclear and can be related to either the transition of CsCl-type to CaF_2-type silicide or the transition from Si- to Co-rich termination. The presence of $1/6 \langle 111 \rangle$ uc steps in combination with 0.4-Å steps is consistent with step heights found on samples where 2 ML of Co were deposited on $CoSi_2$ and annealed at 400 °C [25].

5. Conclusion

In conclusion, we have studied, using UHV-STM, the evolution of ultra-thin Co films on Si(111) 7×7 substrates upon consecutive annealing steps. The small grains that cover the surface after RT deposition transform to trigonal islands that grow laterally upon further annealing. The observed step heights of integer multiples of $1/6$ $\langle 111 \rangle$ of the $CoSi_2$ uc could be best explained by the presence of the recently found cubic CsCl-type CoSi phase. After annealing at 500 °C, a variety

of surface structures are found, including additional steps, with a height of 0.4(1) Å, that separate two different types of surfaces. All these surface features disappear after annealing at 600 °C.

Pinholes appear after annealing at 500 °C. Upon further annealing, their growth leads to a complicated pinhole-induced $CoSi_2$ network that, at temperatures of ~ 700 °C, breaks up into individual islands.

Acknowledgements

References

[1] R.T. Tung, Mater. Chem. Phys. 32 (1992) 107.

[2] H. Von Känel, Mater. Sci. Rep. 8 (1992) 193.

[3] P. Gas, F.M. d'Heurle, Appl. Surf. Sci. 73 (1993) 153.

[4] J.W. Mayer, S.S. Lau, Electronic Material Science for Integrated Circuits in Si and GaAs, Macmillan, New York, 1990.

[5] T. Barge, S. Poize, J. Bernardi, P. Gas, Appl. Surf. Sci 53 (1991) 180.

[6] K.N. Tu, IBM J. Res. Dev. 34 (1990) 868.

[7] K.N. Tu, D.A. Smith, B.Z. Weiss, Phys. Rev. B 36 (1987) 8948.

[8] A. Cros, K.N. Tu, D.A. Smith, B.Z. Weiss, Appl. Phys. Lett. 52 (1998) 1311.

[9] J.M. Gibson, J.L. Batstone, R.T. Tung, Appl. Phys. Lett. 51 (1987) 45.

[10] R.T. Tung, J. Vac. Sci. Technol. A 7 (1989) 599.

[11] C. Pirri, J.C. Peruchetti, G. Gewinner, J. Derrien, Phys. Rev. B 29 (1983) 3391.

[12] F. Arnaud d'Avitaya, J. Cryst. Growth 81 (1987) 463.

[13] J.M. Philips, J.L. Batsone, J.C. Hensel, M. Cerullo, Appl. Phys. Lett. 51 (1987) 1895.

[14] J. Derrien, F. Arnaud d'Avitaya, J. Vac. Sci. Technol. A 5 (1987) 2111.

[15] J.Y. Veuillen, J. Derrier, P.A. Badoz, E. Rosencher, C. d'Anterroches, Appl. Phys. Lett. 51 (1987) 1448.

[16] A.E. Dolbak, B.Z. Olshanetsky, S.A. Teys, Phys. Low-Dim. Struct. 3/4 (1997) 113.

[17] F. Arnaud d'Avitaya, S. Delage, E. Rosencher, J. Derrien, J. Vac. Sci. Technol. B 3 (1985) 770.

[18] P.A. Bennett, D.G. Cahill, M. Copel, Phys. Rev. Lett. 73 (3) (1994) 452.

[19] P.A. Bennett, S.A. Parikh, D.G. Cahill, J. Vac. Sci. Technol. A 11 (4) (1993) 1680.

[20] P.A. Bennett, S.A. Parikh, M.Y. Lee, D.G. Cahill, Surf. Sci. 312 (1994) 377.

[21] C. Pirri, J.C. Peruchetti, G. Gewinner, J. Derrien, Phys. Rev. B 29 (1983) 3391.

[22] J.R. Tucker, C. Wang, T.-C. Shen, Nanotechnology 7 (1996) 275.

[23] G. Palasantzas, B. Ilge, L.J. Geerligs, to be published.

[24] B. Stäuble-Pümpin et al., Phys. Rev. B 52 (1995) 7604.

[25] R. Stalder, N. Onda, H. Sirringhaus, H. von Känel, C.W. Bulle-Lieuwma, J. Vac. Sci. Technol. B 9 (4) (1991) 2307.

[26] S.A. Chambers, S.B. Anderson, H.W. Chen, J.H. Weaver, Phys. Rev. B 34 (1986) 913.

[27] C. Pirri, J.C. Peruchetti, D. Bolmont, G. Gewinner, Phys. Rev. B 33 (1986) 4108.

[28] S.C. Wu, Z.Q. Wang, Y.S. Li, F. Jona, P.M. Marcus, Phys. Rev. B 33 (1986) 2900.

[29] J. Vrijmoeth, A.G. Schins, J.F. van der Veen, Phys. Rev. B 40 (1988) 3121.

[30] D. Hull, D.J. Bacon, Introduction to Dislocations, Pergamon Press, Oxford, 1984.

[31] J.P. Hirth, J. Lothe, Theory of Dislocations, Wiley, New York, 1982.

[32] R. Stalder, H. Sirringhause, N. Onda, H. von Känel, Appl. Phys. Lett. 59 (1991) 1960.

[33] J.A. Kubby, W.J. Greene, Surf. Sci. 311 (1994) L695.

[34] J.A. Kubby, Y.R. Wang, W.J. Greene, Phys. Rev. B 48 (1993) 4473.

[35] J.A. Kubby, W.J. Greene, Phys. Rev. Lett. 68 (1992) 329.

[36] H. von Känel, C. Schwarz, S. Goncalves-Conto, E. Müller, L. Miglio, F. Tavazza, G. Malegori, Phys. Rev. Lett. 74 (1995) 1163.

[37] C. Pirri, S. Hong, M.H. Tuiller, P. Wetzel, G. Gewinner, Phys. Rev. B 53 (1996) 1368.

[38] S. Hong, P. Wetzel, G. Gewinner, C. Pirri, J. Vac. Sci. Technol. A 14 (1996) 3236.

[39] S. Hong, P. Sonnet, L. Stauffer, P. Wetzel, G. Gewinner, D. Bolmont, C. Pirri, Surf. Sci. 352–354 (1996) 617.

[40] F. Hellman, R.T. Tung, Phys. Rev. B 37 (1988) 10786.

[41] F. d'Heurle, C.S. Petersson, J.E.E. Baglin, S.J. La Placa, C.Y. Wong, J. Appl. Phys. 55 (1984) 4208.